

# Detailed mapping of seismic anisotropy with local shear waves in southeastern Kamchatka

V. Levin,<sup>1</sup> D. Droznin,<sup>2</sup> J. Park<sup>3</sup> and E. Gordeev<sup>2</sup>

<sup>1</sup>Rutgers University, 610 Taylor Road, Piscataway, NJ 08854 United States. E-mail: vlevin@rci.rutgers.edu

<sup>2</sup>KEMSD, Russian Academy of Sciences, 9 Piip Bvd, Petropavlovsk-Kamchatsky, Kamchatka, 683006 Russian Federation.

E-mail: ddv@emsd.iks.ru (DD); gord@emsd.iks.ru (EG)

<sup>3</sup>Yale University, 210 Whitney Ave., New Haven, CT 06520 United States. E-mail: jeffrey.park@yale.edu

Accepted 2004 April 15. Received 2004 April 15; in original form 2003 August 11

## SUMMARY

The Kamchatka Peninsula lies over a vigorous subduction zone where Pacific and North American plates converge at a rate of almost 80 mm yr<sup>-1</sup>. Earthquakes associated with the subduction process provide an excellent source of seismic data for the study of anisotropic properties of the upper mantle and crust overlying the downgoing lithospheric slab. We collected a large set of shear waves from events within the slab recorded by a variety of seismic stations in Kamchatka. Data from permanent and temporary networks cover the entire ~700 km length of the subduction zone, with 50–200 km spacing between observing sites, resulting in an unprecedented coverage of the supraslab mantle wedge. We estimated shear wave splitting in selected *S* waves using two techniques and applied quality tests to ensure measurement stability. Fast directions vary from station to station, and they can vary with backazimuth at individual stations and with direction of propagation for individual sources. In over 350 measurements we recovered meaningful splitting delays, up to 1 s, with most delays in the 0.2–0.6 s range. Additionally, in nearly 200 measurements splitting could not be resolved, yielding ‘NULL’ observations. Anisotropic properties of the Kamchatka supraslab mantle wedge vary greatly along the volcanic arc and forearc of the subduction zone. Observed anisotropic indicators in the arc and forearc correlate spatially with some tectonic features (e.g. volcanoes). Inland of the volcanic arc most splitting values indicate trench-parallel fast polarization. We do not observe depth dependence in local *S*-wave splitting delays, consistent with a shallow coherence of anisotropic texture. In the vicinity of Petropavlovsk-Kamchatsky observed anisotropic indicators are coherently trench-normal, and thus consistent with 2-D corner flow. However, splitting above the fragmented slab edge near the Klyuchevskoy volcanic centre is variable and trench-oblique. Birefringence between Petropavlovsk and Klyuchevskoy is weak. Overall, our observations are incompatible with a regional slab-driven corner flow regime.

**Key words:** mantle wedge, seismic anisotropy, shear-wave birefringence, subduction.

## INTRODUCTION

Processes within the region of the upper mantle ‘wedged’ between the overriding and the subducting plates at a convergent margin control one of the most significant ‘products’ of the plate tectonics engine, volcanic arcs, and strongly influence the accretion of continents.

The supraslab mantle wedge is a site of relatively small-scale flow of mantle material. Wedge flow is controlled by the rate, angle and direction of slab descent, the shape of the subducting slab and the nature and behaviour of the overriding plate. The simplest geodynamic model for the mantle wedge is 2-D corner flow driven by shear coupling to the downgoing plate (Ida 1983). Two-dimensional

corner flow is typically prescribed by petrologists to constrain the likely scenarios for metamorphism, volatile release and partial melting in the subduction zone (e.g. Peacock & Wang 1999; Stern 2002). An upper mantle wedge at a convergent margin that deforms in corner flow should develop a trench-normal olivine lattice preferred orientation (LPO) texture detectable by seismic anisotropy studies. Numerical modelling confirms this for trench-normal subduction, a flat slab and an ‘oceanic’ (i.e. thin) overriding plate (e.g. Fischer *et al.* 2000).

Despite the expectations of subduction models, most studies of seismic anisotropy within supraslab wedges do not conform to a simple 2-D corner flow regime. Deviations of the fast wave speed direction from the convergence direction and rapid lateral

variation in indicators appear to be the norm (Ando *et al.* 1983; Yang *et al.* 1995; Margheriti *et al.* 1996, 2003; Fischer *et al.* 1998; Weimer *et al.* 1999; Peyton *et al.* 2001; Smith *et al.* 2001). Locations where fast polarizations are aligned with the direction of slab descent are known (e.g. Izu-Bonin region, Fouch & Fischer 1996), and are not limited to cases where subduction is near-normal to the trench (e.g. central Aleutians, Bender *et al.* 2004). In our survey of the literature such findings appear to be exceptional rather than normal. Such deviations may signify complexities of mantle flow that can develop within a simple regime, such as explored numerically by Hall *et al.* (2000), and empirically by Buttles & Olson (1998). They may also manifest complications in causes of seismic anisotropy, such as the influence of water on olivine deformation (Jung & Karato 2001) or effects of dynamic recrystallization (Kaminski & Ribe 2001). Discriminating between various possibilities is difficult for studies that are limited in lateral (along-arc) extent, either due to scarce dry land suitable for collecting data or to logistical constraints on deployment of ocean-bottom sensors.

In this paper we present a systematic mapping of *S*-wave birefringence from earthquakes that originate in the downgoing slab and are recorded at the surface of the overriding plate. The study covers the entire length (~700 km) of the Kamchatka subduction zone and most of the width of the subducted slab at depth. It makes use of data collected between 1996 and 2001 by a combination of permanent and portable equipment. We devote special attention to the reliability of birefringence estimates, using multiple estimation algorithms and a hierarchical ranking scheme based on the degree of agreement between them. The availability of a reviewed catalogue for local seismic activity provides additional confidence in relating individual observations to specific volumes of the subsurface mantle.

Our main finding is that anisotropic properties of the Kamchatka supraslab mantle wedge vary greatly along the subduction zone, and that they also show systematic changes as a function of distance from the trench. We document strong spatial and directional variations of observed anisotropic indicators and present examples of apparent correlations between anisotropic properties and elements of tectonic framework (volcanoes, configuration of the slab). Overall, our observations do not conform to the expectations of a simple slab-driven corner flow model. Near Petropavlovsk we find a spatially localized region with linear dimensions under 100 km where 2-D corner flow would explain the data well.

## REGIONAL SETTING

The Kamchatka Peninsula overlies a subduction zone where Pacific and North American plates converge at a rate of almost 80 mm yr<sup>-1</sup>. The convergence direction is very close to trench-normal (Fig. 1). Abundant seismicity associated with the subduction process provides an excellent source of data for the study of anisotropic properties in the upper mantle and crust overlying the downgoing lithospheric slab. Gorbатов *et al.* (1997) relocated microseismicity beneath Kamchatka to show that the seismogenic zone dips ~55° from the horizontal along most of the Kamchatka Peninsula, except for the northernmost section where the dip abruptly changes to ~35°. They also showed that the depth extent of the seismogenic zone decreases northwards. In the Kuriles (south of Kamchatka) seismic activity in this subduction zone extends into the mantle transition zone (depths >400 km). The deepest seismicity shallows to 200 km at the junction between Kamchatka and the

Aleutian Arc. Along the Kamchatka subduction zone the seismicity is restricted to the volume characterized by high seismic velocity seen in tomographic images (Levin *et al.* 2002a) suggesting a wholesale disruption of the side edge of the Pacific Slab. Indicators of seismic anisotropy sensitive to upper mantle depths (100–300 km) argue for a major reorientation in mantle fabric near the northern termination of the Pacific Slab (Park *et al.* 2002). These observations were used to infer trench-parallel flow beneath the subducting slab (Peyton *et al.* 2001), with likely lateral flow through the opening where the northern corner of the subducted lithosphere is missing (Levin *et al.* 2002a).

The active volcanic front of Kamchatka follows the 100 km depth contour of the subducting slab, stepping further inland where the slab shallows (Fig. 1). The crust of Kamchatka has continental thickness (~35 km) and seismic velocities well short of 7 km s<sup>-1</sup> (Levin *et al.* 2002b). Both body-wave and surface-wave studies indicate that the upper mantle beneath southeastern Kamchatka is unusually slow (Fedotov & Slavina 1968; Gorbатов *et al.* 1999; Shapiro *et al.* 2000), consistent with a magmatic source region. *Ps* converted phases from teleseismic *P* suggests that strong seismic anisotropy (up to 10 per cent) is associated with the crust–mantle transition region (Levin *et al.* 2002b). The orientation of anisotropic fabric varies throughout the peninsula. At the eastern coast the backazimuth variation of teleseismic receiver functions is consistent with a fast wave speed direction normal to the trench (Levin *et al.* 2002b), but receiver function data at several inland sites favour a more trench-parallel fast wave speed orientation. Previous studies of local shear wave birefringence in Kamchatka (Krasnova & Chesnokov 1998; Luneva *et al.* 2000) use data collected mainly around the city of Petropavlovsk-Kamchatsky (PET in Fig. 1), and so are spatially limited. Both previous studies sought to detect temporal variations in birefringence parameters, and do not interpret the spatial distribution of birefringence in detail. A broad range of fast shear wave orientations is reported in both studies.

On a larger scale, Kaneshima & Silver (1992) and Fischer & Yang (1994) examined source-side anisotropy using birefringence of a small number of *S* waves that left the Kamchatka subduction zone towards stations in North America. The reported directions of fast shear wave speed differ significantly between these two studies, even for the same event–station pairs. Kaneshima & Silver (1992) reported a trench-normal fast direction in splitting from two events. Fischer & Yang (1994) reported trench-parallel alignment of fast wave speed for most events. A study of teleseismic shear wave splitting observed at stations within Kamchatka itself (Peyton *et al.* 2001) showed that stations underlain by the Pacific Slab display coherent birefringence parameters, with fast shear wave speed parallel to the trench. Trench-normal orientation was detected beyond the edge of the slab. Using a small set of measurements on direct *S* waves that showed birefringence inconsistent with that of *SKS* waves, Peyton *et al.* (2001) proposed mantle deformation underneath the slab as the source of the trench-parallel fast shear wave direction in teleseismic *SKS*, and suggested that other fast orientations reflected flow around the slab edge. In the Discussion we test this view in light of our more numerous direct *S* birefringence data.

## METHODOLOGY

An anisotropic medium causes seismic shear waves to split into fast and slow polarizations that tend to align with the symmetry axes of the stress–strain tensor (Crampin 1977), if such symmetry is

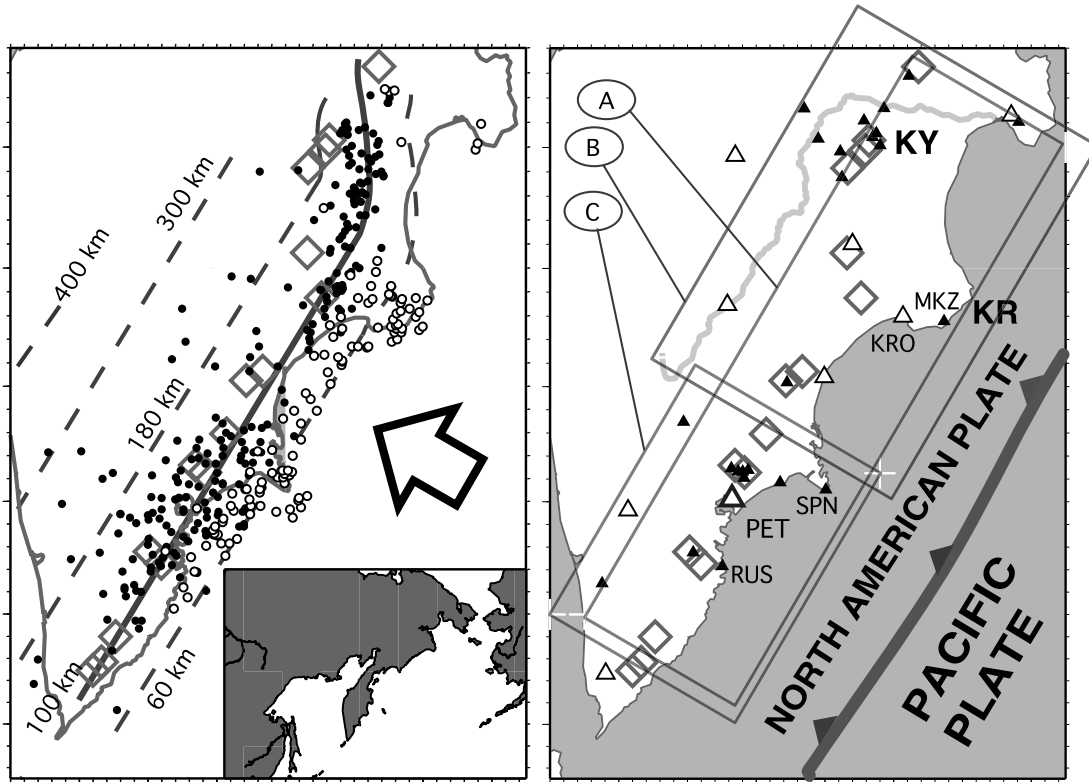


**Figure 1.** (Left) The geometry of the Kamchatka subduction zone. Grey lines, annotated in km, indicate the top of the slab (after Gorbatov *et al.* 1997). A large open arrow shows the direction of motion of the Pacific Plate. Earthquakes used in this study are shown by open (depth less than 100 km) and closed (depth over 100 km) circles. Open diamonds denote active volcanoes. An inset locates the Kamchatka Peninsula within the northern Pacific region. (Right) Short-period stations operated by the Kamchatka Experimental-Methodical Seismological Department are shown by solid triangles, temporary observatories of the 1998–1999 broadband deployment are shown by small open triangles, the Global Seismographic Network site PET is shown by a large open triangle. Stations mentioned in the text are labelled with three-letter codes. Letters mark geographical features: KR, Kronotsky Peninsula; KY, Klyuchevskoy volcanic group. Rectangles denote areas enlarged in Fig. 9 (A) and Figs 4 and 5 (B and C, respectively). A toothed line marks the location of the Kamchatka trench.

present. The time difference between the fast and slow polarizations of the split shear wave accumulate with propagation through an anisotropic medium, depending on ray path length, the intensity of anisotropy and the relative geometry of anisotropy and the ray path. The polarization of fast and slow components of the  $S$  wave is a function of the material properties and the direction of wave propagation through the material.

In a subduction zone,  $S$  waves from events in the slab may be recorded by stations immediately above them, and offer exceptional lateral resolution of birefringence properties. Upon arrival at the receiver, such  $S$  waves carry an integrated signal from the slab, the mantle wedge and the crust. The contributions of various depth regions may be separated if events are observed from a range of depths, and also with the help of external information (e.g. receiver functions, *cf.* Levin *et al.* 2002b). Lateral variability may be probed with rays that sample distinct volumes of rock, and also with rays that sample similar rock volumes in different directions.

### Data selection

We collected a large ( $\sim 700$  source–receiver pairs) set of shear waves from events within the subducting slab recorded by a variety of seismic stations in Kamchatka. Data sources included the permanent broadband seismic observatory PET in Petropavlovsk-Kamchatsky,

a regional network of digital short-period seismic stations and a temporary network of broadband seismic observatories operated in Kamchatka during 1998–1999 (Fig. 1). We mitigated differences in sensor performance by imposing similar bandpass filters on all data. In addition, data from short-period sensors were corrected for the instrument response prior to filtering. A typical bandpass used was 0.5–2 Hz, although some data recorded by broadband stations allowed a lower bandpass (0.1 to 1 Hz).

The catalogue of seismicity compiled by the Kamchatkan Experimental-Methodical Seismological Department (EMSD hereafter, see <http://www.emsd.iks.ru>) was used as a basis for selecting events for the study. Selection criteria included event size, depth and distance from the station, and the quality of the hypocentral location. For long-running stations (the GSN node PET and stations of the regional short-period network) we used events larger than energy class 9 (as defined by EMSD) in a time interval from 1996 to 2001. For stations of the temporary broadband deployment in 1998–1999 (see Fig. 1) we searched all entries in the catalogue. We used waveforms that arrived at the surface with an incidence angle of less than  $35^\circ$ , and originated from hypocentres deeper than 35 km (i.e. beneath the crust, *cf.* Levin *et al.* 2002b) and located to within 10 km, both in depth and laterally. Further selection of records for the analysis was performed on the basis of visual assessment of signal-to-noise level and waveform clarity. Fig. 2 presents examples of observed seismograms, some with obvious birefringence and others with an equally obvious lack of it.

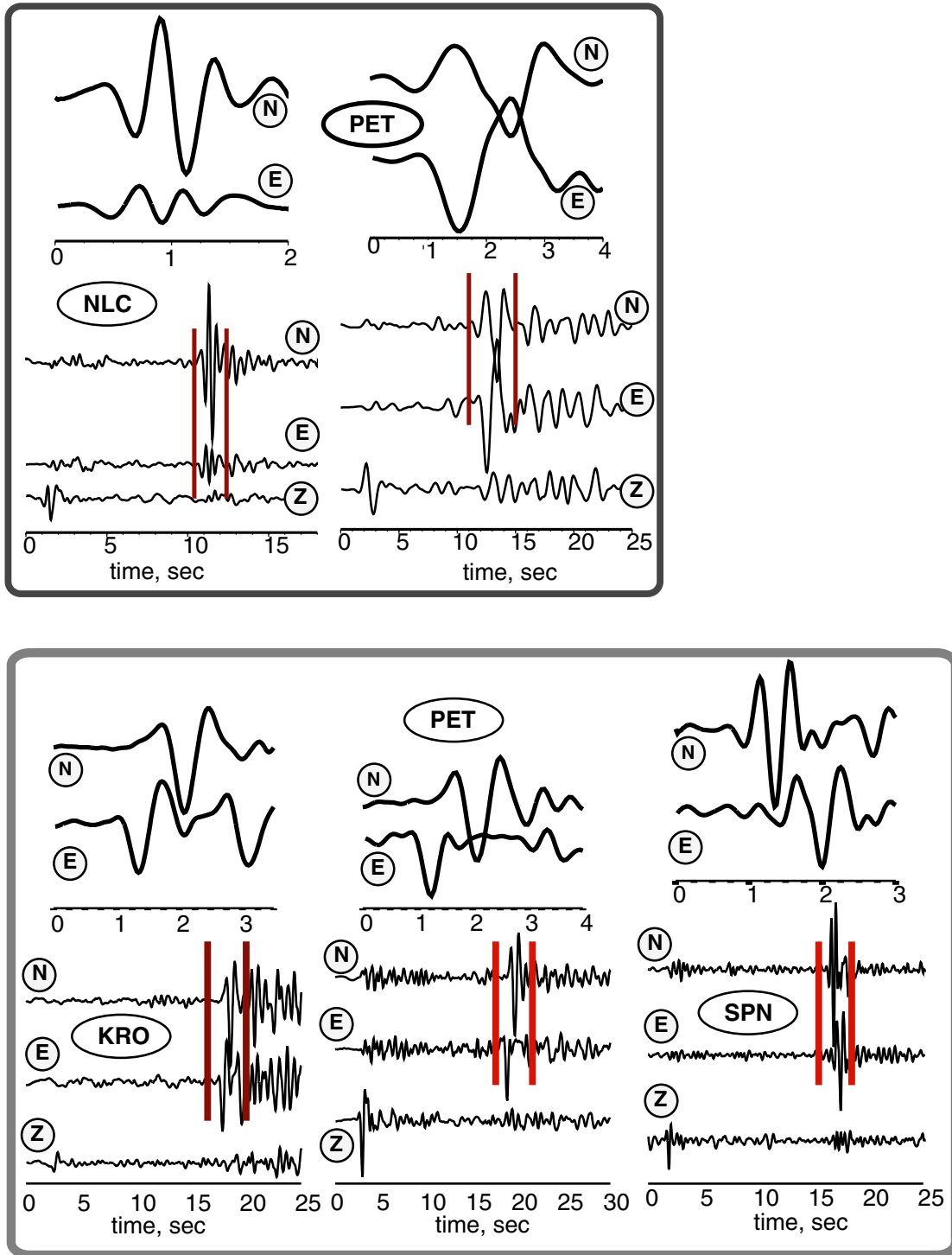


**Figure 2.** Examples of observed waveforms, from broadband and short-period sensors. (Top) Two examples of  $S$  waves with rectilinear particle motion. Upper plots show enlarged waveforms between vertical bars on the lower plot. Note the nearly exact coincidence of peaks and troughs on both horizontal components. Horizontal axes are in seconds. (Bottom) Three examples of naturally rotated  $S$  waves, with clear birefringence. Delays between fast and slow components of the  $S$  wave are as large as 1 s.

### Data analysis

Our analysis methodology assumes that each observation represents shear wave propagation through a medium with constant anisotropic properties. Consequently, shear waves are assumed to be initially polarized in a single plane, and having been ‘split’ only once. Under

these assumptions it is possible to describe the effect of anisotropy by a combination of a single fast polarization azimuth ( $\phi$ ) and a single delay ( $\Delta t$ ) between the fast and the slow components. This last point is critical, since propagation of shear waves through multiple regions of seismic anisotropy leads to a cumulative birefringence of particle motion which can be described by a single pair

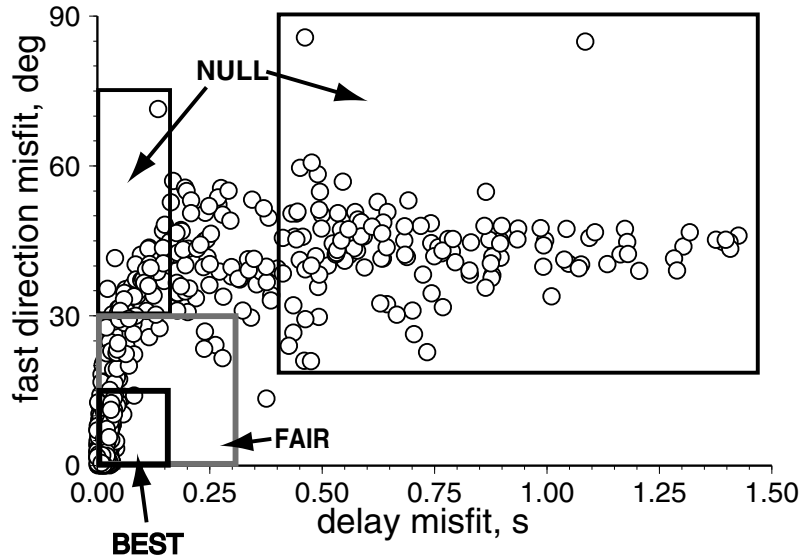


**Figure 3.** A diagram comparing splitting values determined for each observation by two different techniques. Differences in values of  $\phi$  and  $\Delta t$  are used to assign quality (BEST or FAIR), to define NULL observations, and to exclude some observations (symbols outside the boxes). See text for details.

of  $\phi$  and  $\Delta t$  only in an ‘effective’ manner (Silver & Savage 1994; Rumpker & Silver 1998; Levin *et al.* 1999; Saltzer *et al.* 2000). The latter scenario is quite plausible in a subduction zone, and thus our measurement values are not necessarily representative of any one anisotropic system. Rather they must be examined in the context of specific ray propagation geometry. Thus, it is not surprising for the same volume sampled in different directions to yield effective splitting parameters that disagree. We note that a similarity of splitting values (at least in terms of the fast direction) for different ray paths within the same volume would suggest a single source of splitting within the volume. In such cases we can treat observed values of birefringence as representative of the true anisotropy-inducing fabric. This reasoning informs our choice (in subsequent sections) of referencing individual observations to the midpoint of a ray connecting a source and a receiver, rather than to either specific sources or specific receivers.

We use two different techniques to estimate shear wave splitting in each analysed  $S$  phase. The first method rotates the horizontal components to yield waveforms on the two components that are most similar, and then estimates the delay between them via cross-correlation (e.g. Ando *et al.* 1983; Bowman & Ando 1984; Levin *et al.* 1999). The second method seeks a combination of a rotation and a delay which, once it is used to correct for the effect of anisotropy, would minimize one of the components of motion (Vinnik *et al.* 1984; Silver & Chan 1991). Using two measurement algorithms together mitigates against technique-specific biases in the analysis of noisy data (e.g. Menke & Levin 2003; Levin & Okaya 2003). Observations yielding low values of cross-correlation were also checked for dependence on small changes in bandpass filter parameters. Most data records were from short-period instruments, so we did not attempt to resolve the dependence of birefringence on the passband. Rather, we excluded observations with strong frequency dependence from further analysis. Our final data set includes 619 individual observations from source–receiver pairs.

We use values of  $\phi$  and  $\Delta t$  determined by the two splitting estimators to rank the quality of observed birefringence parameters, as follows: BEST measurements yield values of  $\phi$  that agree to within

$15^\circ$  and values of  $\Delta t$  that agree to within 0.15 s; FAIR measurements yield values of  $\phi$  that agree to within  $30^\circ$  and values of  $\Delta t$  that agree to within 0.3 s. NULL measurements (i.e. no resolvable splitting) are defined by: (1) both measurement techniques yield  $\Delta t < 0.05$  s; or (2) one method yields  $\Delta t < 0.1$  s, while the other method yields  $\Delta t > 0.5$  s, and there is a large ( $>35^\circ$ ) disparity in values of  $\phi$ . The second criterion is based on our experience with both synthetic and real split shear waves. For cases of low signal to noise ratio, Menke & Levin (2003) shows that the cross-correlation method tends towards smaller delays, while the technique based on energy minimization on one component favours the maximum delay allowed in a search. A similar effect is seen in synthetic seismograms in complex anisotropic structures (Levin & Okaya 2003). Measurements that do not fit in the above three categories (66 observations in total) are not used further. Overall, the selection process described above yields 303 measurements of BEST quality, 59 measurements of FAIR quality and 191 NULL measurements. Comparing lateral and depth distributions of events that were included in the final selection, and those 66 that were excluded, we find nothing special about the latter set. The high discrepancy in values of splitting parameters that leads to the exclusion of these observations may stem from higher noise levels in individual records or else reflect the source complexity of specific events. Fig. 3 shows the distribution of  $\phi$  and  $\Delta t$  misfits between two measurement methods, and illustrates definitions of quality classes (BEST, FAIR, NULL).

The above ranking scheme used splitting parameters returned by two measurement algorithms, and did not take into account the error in those values. As described in more detail in the Appendix, we found the formal error of the measurements to be a poor predictor of whether a particular observation will fall into one of the three categories above. We believe that the bounds used for ranking provide a better estimate of the uncertainty in observations. We estimate the BEST measurements errors to be one-half of respective bounds, that is, 0.075 s for the delay and  $7.5^\circ$  for the fast direction. For FAIR observations these values are 0.15 s and  $15^\circ$  respectively.

## RESULTS

### Overview

Figs 4 and 5 show a synoptic view of shear wave splitting measurements above the Kamchatka subduction zone. To clarify the affinity of individual measurements, we plot them using the following procedure. Each pair of  $\phi$  and  $\Delta t$  values that represents an individual measurement is depicted by a bar, scaled with delay and aligned with the fast direction. The spatial position of each bar is determined from the depth and location of the source. We assume propagation along a straight ray and determine the horizontal position of the ray's midpoint, to which we assign the measurement. In plotting individual measurements, we colour them according to the depth of the midpoint. This way we get a first-order sorting of measurements in accordance with the volumes they sample.

Taken together, our measurements display a remarkable diversity of  $\phi$ - $\Delta t$  combinations. Encouragingly, there are some regions of conspicuous similarity in measurements. They reaffirm the notion that distinct anisotropic indicators represent properties of specific regions in the Earth. Also, they allow us to examine relationships between anisotropic indicators and tectonic features.

### Pattern of averaged splitting indicators

Most of our observations, when projected to midpoints of their respective rays, fall between depths of 50 and 100 km (Fig. 6), making this depth interval the best sampled. Fig. 7 shows results of averaging all BEST measurements that fell within this depth range. We use a lateral window  $0.5^\circ$  wide, with 50 per cent overlap, and plot resulting values for all lateral bins that enclosed four or more measurements. The averaging scheme treats splitting observations as vectors within the  $(\phi, \Delta t)$  plane, and averages values according to the 'length' of individual pairs. Averaged anisotropic parameters identify regions of coherent orientation with greater clarity. Spot-checks confirm that averaged orientations are consistent from maps of raw measurements (Figs 4 and 5).

We have dense observations of shear-wave splitting in two regions along the volcanic front of Kamchatka: in the vicinity of the city of Petropavlovsk-Kamchatsky and between the Kronotsky Peninsula and the Klyuchevskoy group of volcanoes. The gap between these two groups of averaged indicators is largely due to the paucity of observations. It is notable, however, that measurements here (Fig. 5) display weak splitting, or else were designated as 'NULL', i.e. no resolvable signal could be extracted.

Within the southern cluster of averaged indicators ( $52^\circ$ – $53.5^\circ$ N) many fast directions align in the trench-normal direction beneath the volcanic arc, and appear to be trench-parallel further inland. The pattern is broken up wherever volcanoes are present, especially in the northernmost part of the cluster, where many splitting directions are oblique to the trench, and display NNW orientation. Also notable are inland bins where splitting has fast polarization that is consistently trench-parallel.

Within the northern cluster ( $54.5^\circ$ – $56^\circ$ N) two fast directions are prevalent, both oblique to the orientation of the trench. At the coast and beneath the Klyuchevskoy group of volcanoes, fast directions trend northwards ( $\pm 15^\circ$ ), while a region in the centre of the cluster shows some bins with a coherent northeast fast direction.

A notable feature of the averaged splitting map is the modest size of the splitting delay, 0.5 s and less. The averages are consistent with the distribution of splitting values in the raw data set (Fig. 8).

The average ray length (100–200 km) and a delay of 0.5 s implies between 1 and 3 per cent average anisotropy along the ray. This inference is confirmed if a ratio of delay to ray length is taken for all observations. Values of this ratio do not exceed  $6 \times 10^{-3} \text{ s km}^{-1}$  (seconds of delay per kilometre of ray path). For mean  $V_s = 4.4 \text{ km s}^{-1}$  this translates into ray-averaged anisotropy under 3 per cent.

### Small-scale structure

Data from the long-running seismic observatory PET combines data streams from the broad-band sensor that is part of the Global Seismic Network and the short-period sensor operated by the EMSD. We found no systematic differences between measurements in data from the two sensors. PET data exhibit a correlation between observed shear wave splitting measurements and features of the local tectonics (Fig. 9). There is a marked change in splitting values and orientations between the area to the southwest of the station (marked by a solid circle) and the area to the northeast of it. Within the southwest area most observations yield relatively large values of splitting, with fast directions close to trench-normal alignment. Most observations that sample this area are ranked BEST. Within the northeast area, splitting values are generally smaller (with a few notable exceptions), there are numerous FAIR observations and a sizeable fraction of NULL observations. The most obvious distinction between the two areas sampled by seismic waves is the presence of a major volcanic centre to the north of PET. Two active volcanoes within this centre are marked by diamonds in Fig. 9.

### No depth dependence in delay magnitude

Reports of depth dependence of seismic anisotropy intensity in the supraslab mantle of subduction zones are common (Yang *et al.* 1995; Fouch & Fischer 1996; Audoine *et al.* 2000). Figs 10 and 11 present lateral and depth distributions of splitting observed for a few stations on the eastern coast of Kamchatka. Because of their proximity to the trench, these sites have both large numbers of observations (smaller earthquakes are visible clearly) and a broad spread of depths. We do not see a clear dependence of the splitting value ( $\Delta t$ ) on depth (see Fig. 12), and NULL measurements also appear to be evenly distributed over the depth interval sampled.

## DISCUSSION

Lacking direct measurements, we must infer mantle flow in the subduction zone mantle wedge from proxy geophysical observations. Of particular interest are seismological observations that may be interpreted in terms of elastic anisotropy. Upper-mantle seismic anisotropy is thought mainly to be caused by systematic alignment of the LPO of strained olivine crystals, and is thus related to mantle deformation processes (see reviews by Silver 1996; Savage 1999; Park & Levin 2002). In dry upper mantle peridotite a fast direction develops from the alignment of the *a* axes of olivine crystals (Christensen 1984; Ben-Ismaïl & Mainprice 1998). The orientation of this crystallographic axis reflects, to first order, the direction of solid flow in the material (Zhang & Karato 1995; Kaminski & Ribe 2001). In the supraslab mantle wedge, seismic anisotropy may reflect other mechanisms as well, in particular the presence of melt distributed throughout the volume (Holtzman *et al.* 2003), or else present in the form of pockets and networks (Aharonov *et al.* 1995; Korenaga & Kelemen 1998). It may also be sensitive to the presence of water (Jung & Karato 2001).

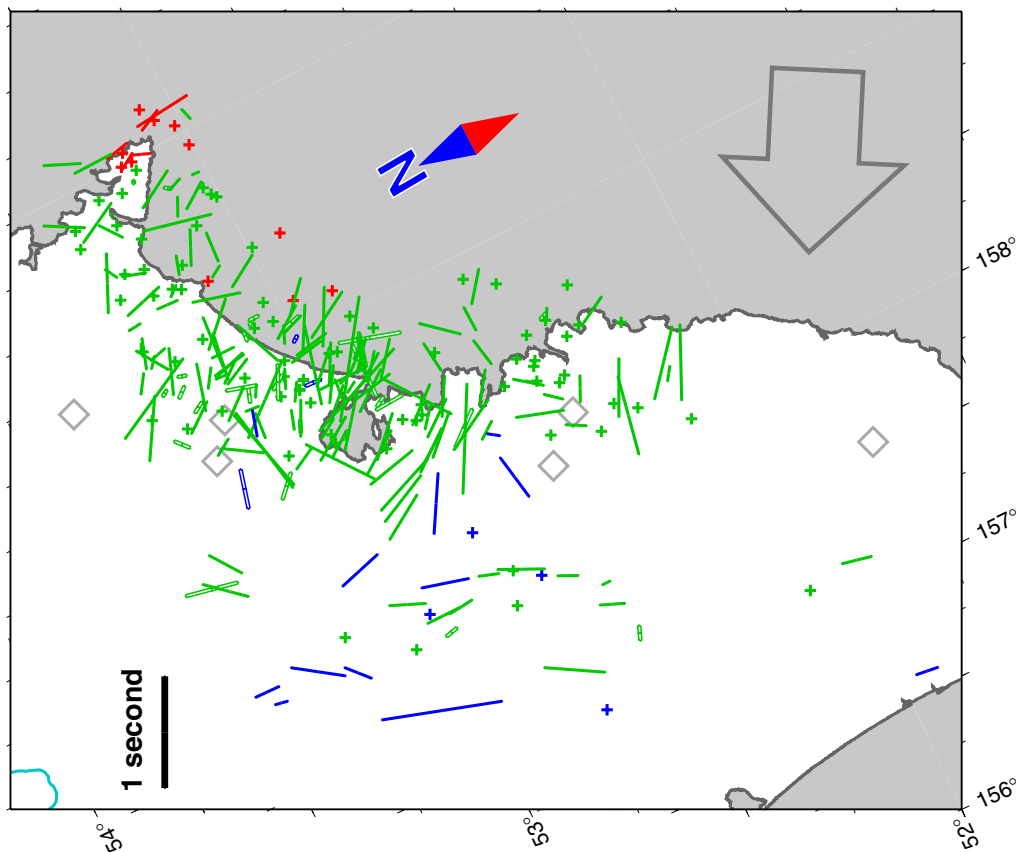


**Figure 4.** Shear wave splitting observations in the southernmost Kamchatka Peninsula. Individual observations are mapped at horizontal projections of midpoints along rays connecting earthquakes and stations. Bars are oriented with the apparent fast polarization, and are scaled with the value of the delay. Solid bars represent BEST measurements, open bars represent FAIR measurements. A solid bar in the upper left corner of the plot is equivalent to a 1 s delay. Crosses show NULL measurements. Observations are colour coded by the depth of the ray midpoint. Colour (shades of grey) in electronic (print) versions are as follows: red (light grey), above 30 km; blue (black), below 100 km; green (dark grey), between 100 and 30 km. Open diamonds show locations of active volcanoes. A large open arrow shows the subduction direction of the Pacific Plate.

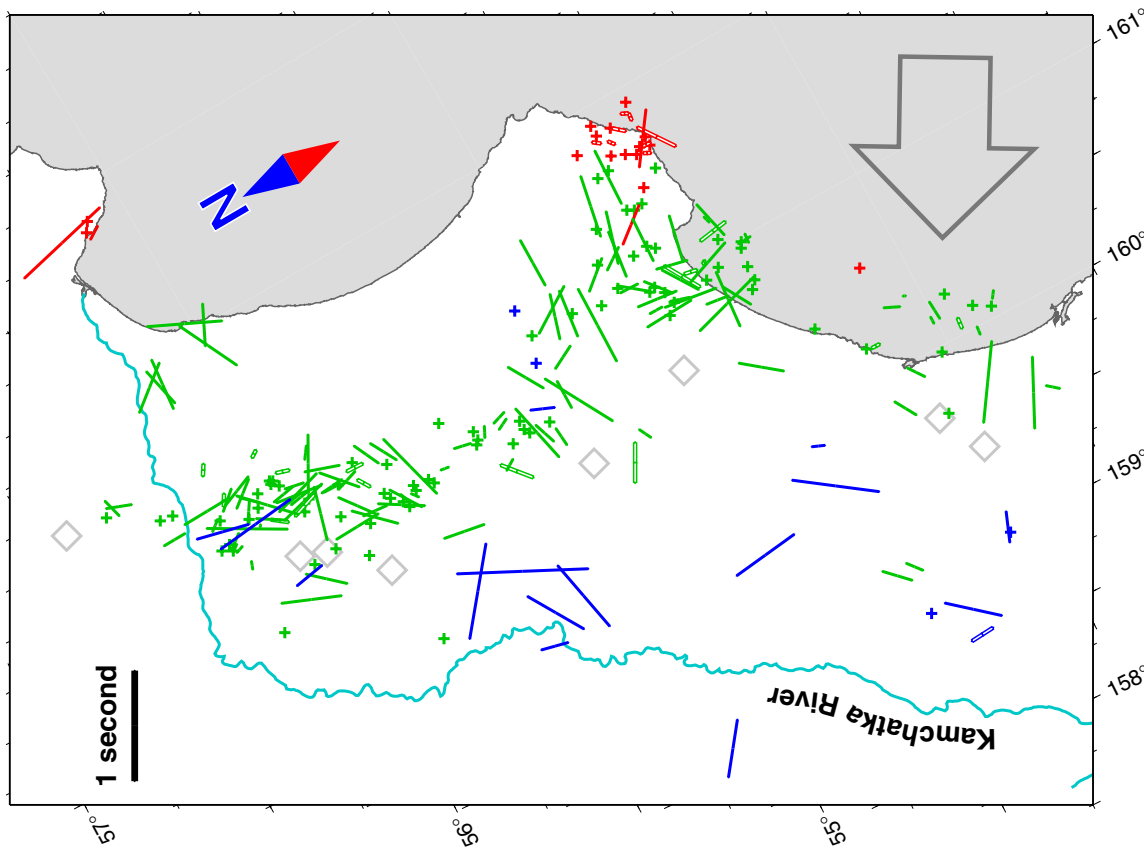


**Figure 5.** Same as Fig. 4, for the central Kamchatka Peninsula, including the Kamchatka–Aleutian junction.

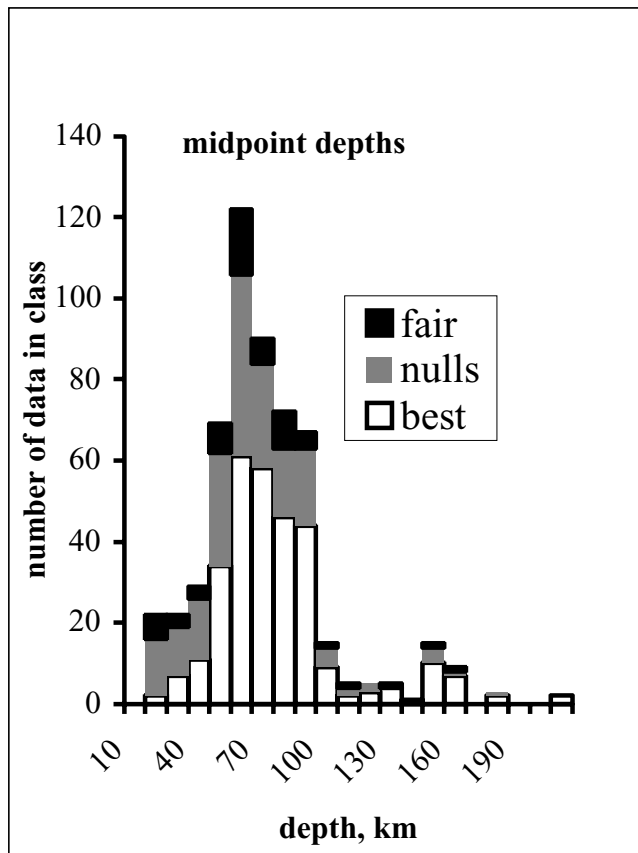


**Figure 6.** Depth distribution of ray midpoints for observations used in this study.

Furthermore,  $S$  waves ascending through the subduction zone accumulate an anisotropic signal from the slab, the mantle wedge and the crust. As a result, observed quantities ( $\phi$  and  $\Delta t$ ) become complex functions of the wave propagation direction, the original polarization of  $S$  waves and the structure the wave has sampled (Rumpker & Silver 1998; Saltzer *et al.* 2000).

Birefringent  $S$  waves observed in Kamchatka offer a dramatic illustration of the above complexity. We see clear birefringence, and can recover fast directions ( $\phi$ ) and delay values ( $\Delta t$ ) for a large number of observations. However, on a scale of the entire subduction zone it is hard to categorize observed patterns in broad terms of a single simple model, such as 2-D corner flow or uniform trench-parallel flow. Rather, anisotropic indicators appear coherent in relatively compact areas beneath Kamchatka. We also find areas where individual anisotropic indicators display great scatter, and at least one area (south of the Kronotsky Peninsula) where most anisotropic indicators are NULL or else show very small  $\Delta t$  values.

The significant lateral variability in seismic anisotropy indicators in the Kamchatka data set is important. Most shear-wave splitting studies in oceanic subduction zones suffer from sparse data, either due to limitations of siting seismometers on oceanic islands or else due to limitations on the time of operation of ocean-bottom sensors. If the variability of properties beneath Kamchatka is common among subduction zones, great caution should be exercised in interpreting results of space- and time-limited studies. In a similar vein, our finding that splitting parameters in local  $S$  waves suffer from technique-specific bias points to the danger of over-interpreting sparse individual observations of birefringence. The cross-verification scheme adopted in this paper offers us extra confidence in the values that are

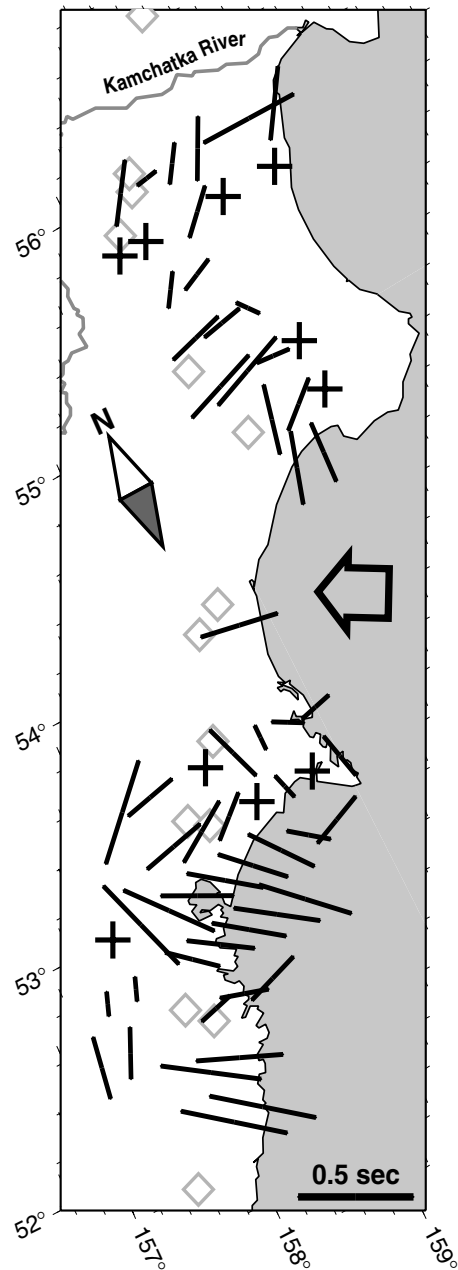


**Figure 7.** Averaged shear wave splitting measurements projected to midpoints along their respective rays. All observations that project to the depth between 50 and 100 km are averaged in spatial bins  $0.5^\circ$  wide, with 50 per cent overlap between bins. Bins with four or more observations are plotted. Bars representing splitting measurements are aligned with the fast direction, scaled with delay, and registered to the centre of the bin. Crosses denote bins where averaged delay fell below 0.1 s. An open arrow shows subduction direction of the Pacific Plate. A compass sign (shaded to the south) is included for reference.

independent of technique, and also protects us from anxiety about outliers in data.

One other methodological issue essential for studies of shear wave splitting in local  $S$  waves is the meaning of the NULL measurements. In this paper we adopted a practical definition of a NULL, based not just on the size of the delay but also on the discrepancy between two techniques (Fig. 3). A recent survey of the performance of the shear wave splitting techniques by Menke & Levin (2003)

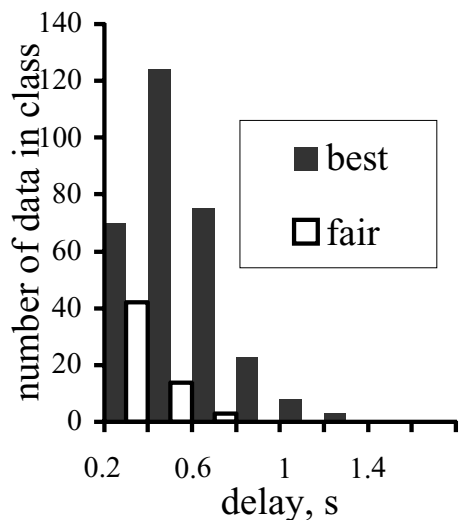


**Figure 8.** Distribution of delay values in the Kamchatka local *S* birefringence data set.

informed our definition. In the Kamchatka data set nearly a third of the observations yielded NULL measurements. Unlike the teleseismic *SKS* phase which is naturally polarized in the radial plane, a direct *S* wave has an initial polarization that depends on the source mechanism of the earthquake. There is no source mechanism information for the small earthquakes beneath Kamchatka that we use in this study. Consequently, the physical meaning of NULL measurements in our data is less straightforward than in studies of teleseismic core-refracted phases. In addition to the null hypothesis of no anisotropy, and the case where the ray direction coincides with one of the anisotropic symmetry axes, we must consider cases where the initial polarization of the *S* wave lies in the plane of one of the

symmetry axes. There is also a possibility that two (or more) distinct anisotropic regions were sampled, and have yielded a mutual cancellation of birefringence (Saltzer *et al.* 2000; Menke & Levin 2003). In view of this uncertainty we did not incorporate NULL observations while deriving averaged values of birefringence (Fig. 7).

With all the caveats discussed above, we can examine the pattern of seismic anisotropy indicators and compare it with expected behaviours, and with previous findings for the region. Comparing the present study to Krasnova & Chesnokov (1998) and Luneva *et al.* (2000), all studies report considerable scatter in the apparent fast polarizations of local *S* waves. Both previous studies report a preference for an east–west fast direction at the station PET, but also a scattering of other alignments. Comparing these findings with ours (Fig. 9) we note that both east–west and north–south fast directions are present in the data set observed at PET, primarily for hypocentres east of the station. Notably, most hypocentres southwest of PET yield a different (northwest–southeast) fast direction that is close to trench-normal. A plot in Krasnova & Chesnokov (1998) (their Fig. 1) also shows that two sites nearest to the trench have many observations with nearly north–south fast polarizations, compatible with our findings (Fig. 9). The primary difference between our study and the two previous ones stems from assumptions about the mechanism of anisotropy. While we emphasize LPO in mantle rocks, both Krasnova & Chesnokov (1998) and Luneva *et al.* (2000) assume that anisotropy in the crust reflects crack systematics. They ascribe differences in directions of fast shear wave speed to dynamic changes in the state of the crustal rock mass, and relate it to preparatory cycles of regional earthquakes. No consideration is given in either of these studies to the dependence of splitting measurements on the backazimuth of the incoming shear wave, so the interpretation of time-variable splitting is ambiguous. Backazimuthal variation related to seismicity distribution in space offers an alternative explanation for (apparent) temporal changes in splitting values observed at individual stations. Our work on teleseismic *Ps*

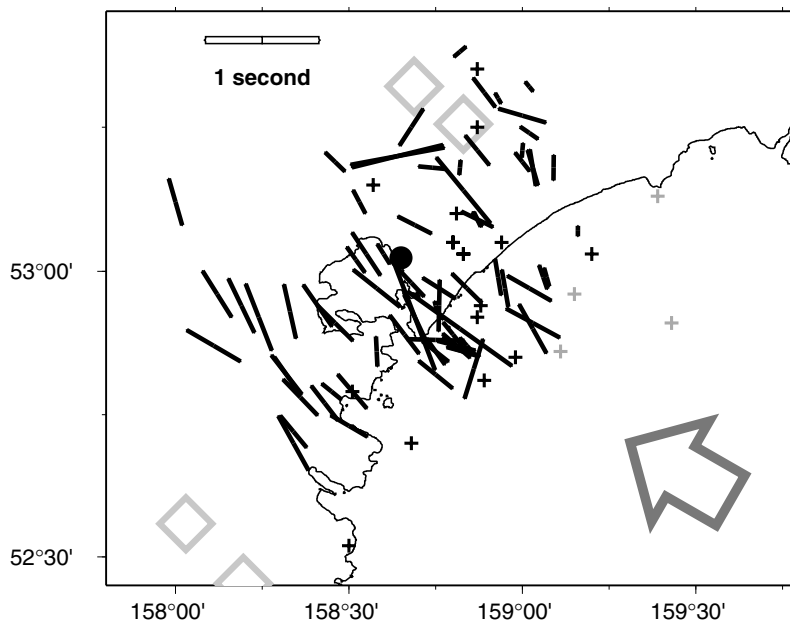


**Figure 9.** Shear wave splitting observations for station PET (solid circle). Individual observations are mapped at horizontal projections of midpoints along rays connecting earthquakes and stations. Bars are oriented along the fast direction, and are scaled with the value of the delay. An open bar in the upper left corner of the plot is equivalent to a 1 s delay. Crosses denote NULL measurements. Observations for which midpoints of rays are above 30 km depth are shaded, those with deeper midpoints are solid. Open diamonds show locations of active volcanoes. A large open arrow shows the subduction direction of the Pacific Plate.

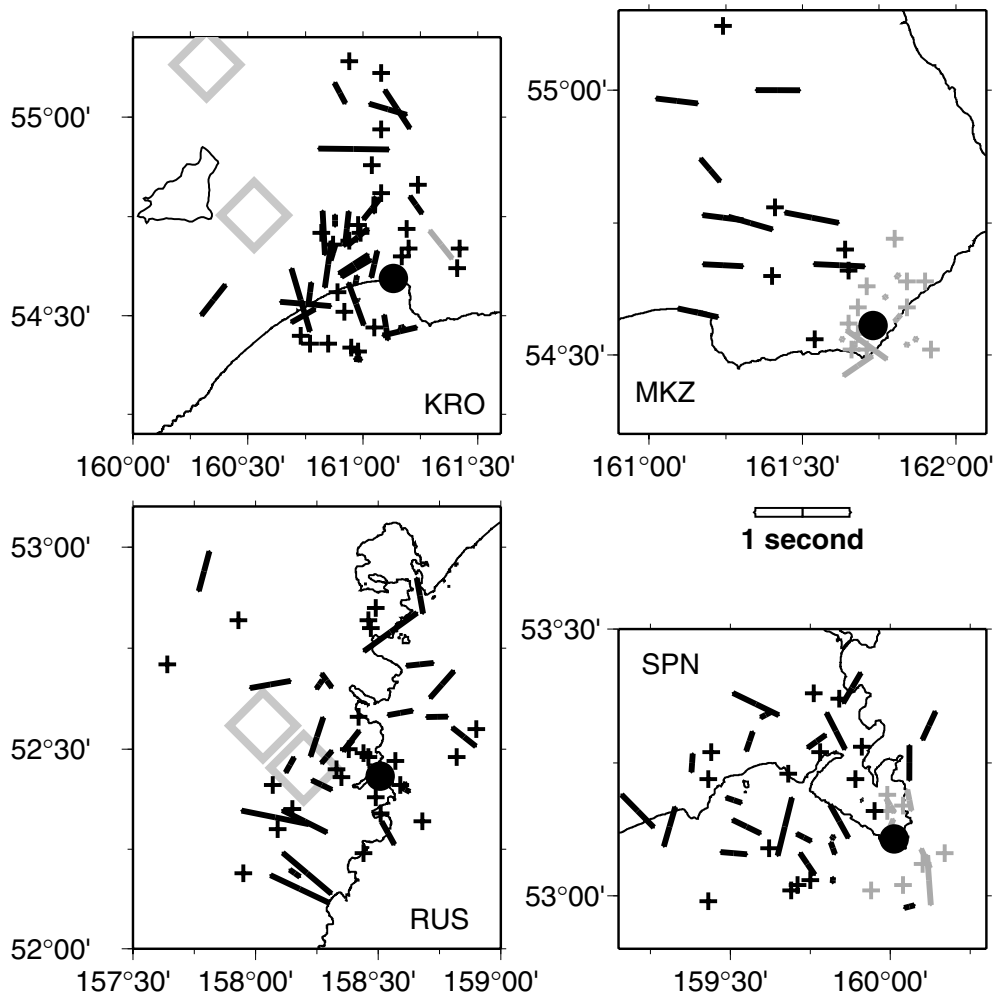


**Figure 10.** Shear wave splitting observations at a number of sites with large ranges of observed source depths. Symbols are as in Fig. 9. An open bar between panels for stations MKZ and SPN is equivalent to a delay of 1 s.

phases with receiver functions (Levin *et al.* 2002b) demonstrated the need for anisotropy in the mantle beneath Kamchatka.

A study of teleseismic *Ps* body waves (Levin *et al.* 2002b) yielded evidence for anisotropic fabric beneath Kamchatka, especially in the depth range of the crust–mantle transition (30–50 km). Unlike birefringent *S* waves, *P-SH* mode-converted phases are sensitive to the location of strong gradients in anisotropic properties, and can be used to constrain depth. As discussed in Levin *et al.* (2002b), the interpretation of receiver functions in terms of actual anisotropic material at depth is often contingent on assumptions about the symmetry and the sense of the axis (fast or slow). Along the eastern coast of Kamchatka, that study also reported trench-normal fast directions of shear wave speed, while in the interior fast directions varied. In all cases the depth region where anisotropy was required in models did not extend below 70 km.

At face value, the lack of depth dependence in shear wave splitting delays (Fig. 12) would support the notion that the bulk of anisotropy is located close to the surface. However, our measurements probably represent ‘effective’ anisotropy (see section on Data Analysis), so we do not stress this inference here. In the future we plan to conduct a direct comparison of our *S*-wave birefringence measurements with predictions from models based on mode-converted waves.

Teleseismic *SKS* splitting investigated by Peyton *et al.* (2001) indicates trench-parallel fast shear wave directions in the area underlain by the Pacific Slab. Local *S* waves yield different fast polarizations along the eastern shore of Kamchatka (Fig. 7). There is, however, a region in the interior where most splitting indicators show fast direction approximately along the trench (Fig. 4). These measurements are obtained from deepest slab earthquakes in Kamchatka, for which a sizeable fraction of the ray path could be within the subducting plate. Peyton *et al.* (2001) examined a few weakly split local *S* waves observed near the coast, and concluded that the *SKS* signal must reflect the state of either the slab or the slab mantle. Our new measurements would be consistent with the involvement of the slab in some instances of local *S* birefringence. However, a similar trench-parallel alignment in the anisotropy inferred from receiver functions at some inland stations (Levin *et al.* 2002b) suggests that this trench-parallel local *S* birefringence may originate in the shallow mantle. Scenarios involving the trench-parallel flow within the supraslab mantle wedge have been previously proposed for the Tonga subduction zone by Smith *et al.* (2001) and for the South Sandwich Arc by Leat *et al.* (2000). Evidence for such flow in an exhumed arc is reported by Mehl *et al.* (2003).

Overall, our present findings and those from other studies characterize the upper mantle and crust of southeastern Kamchatka as

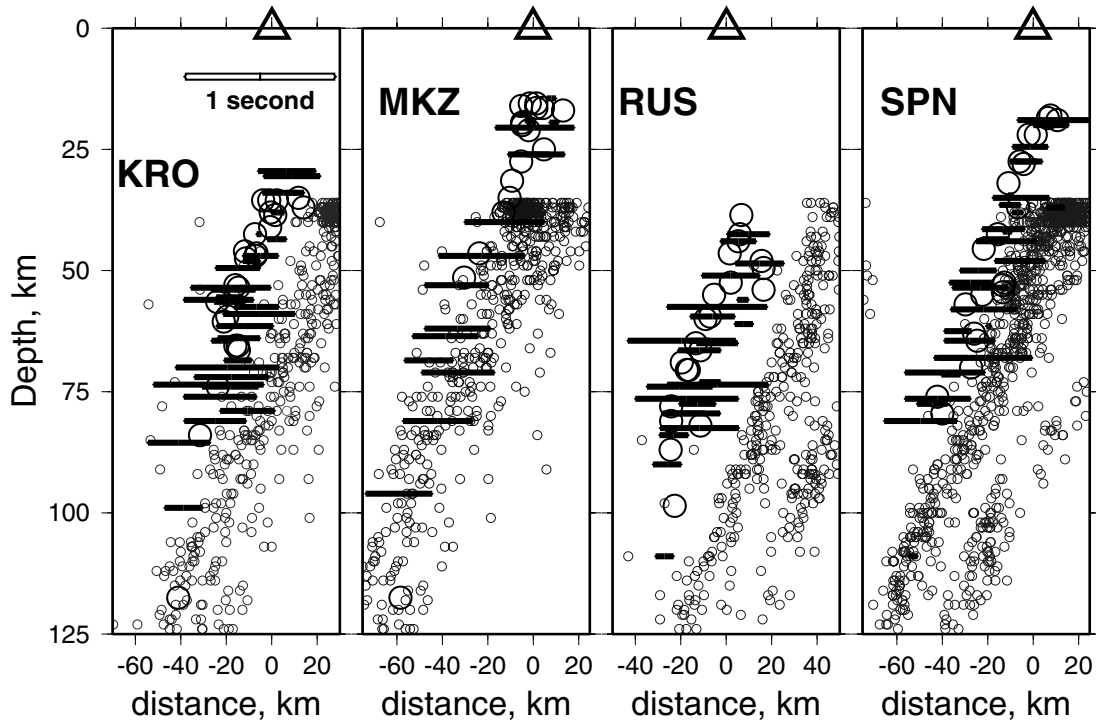


**Figure 11.** Splitting delay values (horizontal bars proportional to delay value) and NULL measurements (solid circles) for stations KRO, MKZ, SPN and RUS are referenced to ray midpoints and projected onto a trench-normal vertical planes passing through stations. Small grey circles show all seismic sources in the EMSD catalogue within 50 km of the cross-section plane that are located to within 10 km, and have hypocentres below 35 km. Open triangles show relative positions of respective seismic stations.

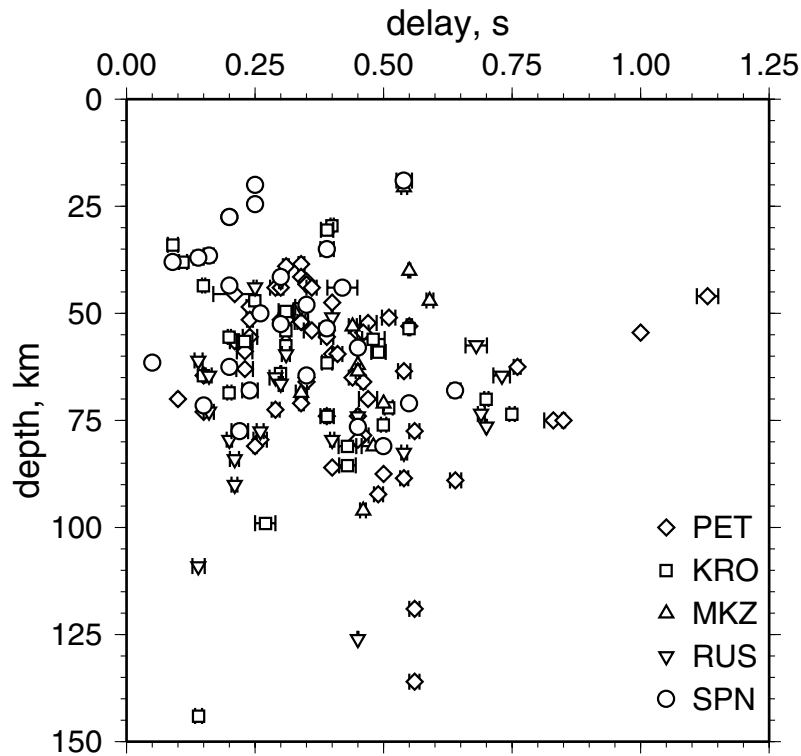


**Figure 12.** Delay values for seismic stations that have measurements from broad ranges of source depths. Symbols are as indicated on the plot. Error bars denote half-values of misfit between two measurement techniques. No depth dependence is apparent, either in single-station data or in a cumulative data set.

a region with complex distribution of anisotropic properties, with lateral and depth variations of anisotropy on relatively short (tens of kilometres) scales.

Our results provide further support for the conclusion by Peyton *et al.* (2001) that trench-parallel flow takes place beneath the Kamchatka Slab. Peyton *et al.* (2001) compared birefringence in *SKS* phases (which they found to be very coherent in southeastern Kamchatka) and that of a few direct *S* waves (which showed considerable scatter). Our present study of a large set of direct *S* waves confirms the diverse character of local *S* birefringence.

Our Kamchatka study identifies features similar to those found in other studies in subduction environments, though there are contrasts. An early study of seismic anisotropy in Japan (Ando & Ishikawa 1980; Ando *et al.* 1983) identified localized areas characterized by seismic anisotropy, with fast polarization that varies laterally and splitting delay values approaching 1 s. A later study that used broad-band data (Fouch & Fischer 1996) also found lateral variation in splitting values. The pattern of fast directions reported by Fouch & Fischer (1996) for central Honshu appears similar to the one we find in the southern part of Kamchatka: the fast polarization is approximately aligned with the subduction direction for observations close to the trench, while further from the trench the fast polarization rotates to nearly trench-parallel orientation.

A study of Smith *et al.* (2001) in the Tonga subduction zone also finds laterally variable fast polarization, and delays upwards of 1 s. Of note is a reversal of the pattern of fast directions, relative to our study: close to the trench. Smith *et al.* (2001) find trench-parallel fast directions, while in the backarc region the predominant fast direction is close to trench-normal. This difference could be related to the nature of the overriding plate. In the case of Tonga the upper plate is oceanic, and there is an active backarc extension region. The Kamchatka Peninsula is continental in its seismic structure. However, there are other subduction zones with continental overriding plates where birefringence in local *S* waves suggests a predominantly trench-parallel fast direction: the segment of the Aleutian Arc studied by Yang *et al.* (1995), the North Island of New Zealand (Audoine *et al.* 2000) and parts of Japan (Shimizu *et al.* 2003). Also, Polet *et al.* (2000) report a reorientation of fast directions, from trench-parallel close to the plate boundary to trench-normal further away, beneath the central segment of the South American subduction zone.

Given a multitude of potential contributing factors like the thick crust (of the South American Altiplano), the oblique subduction vector (in the Aleutians) and the complex morphology of subducted plate (beneath Japan), a single global cause controlling the nature of the fast-direction pattern probably does not exist. From the small survey of reported localities, the Kamchatka/Honshu splitting pattern appears less common, but this distinctiveness may change once more convergent margins are explored in detail.

### Evidence for corner flow in the wedge?

Simple slab-driven corner flow in a subduction zone should produce a trench-normal fast polarization. On the scale of the entire Kamchatka subduction zone this is not observed (Figs 4 and 5). Rather, we can identify specific regions (e.g. an area south of Petropavlovsk-Kamchatsky), where corner flow would be consistent with observations (Fig. 9). Given the diverse mechanisms in the formation of the olivine LPO and shear wave birefringence observations, a broad-scale corner flow cannot be ruled out altogether. It is possible that there is indeed a large region of the Kamchatka mantle

wedge where strained mantle rocks develop LPO with trench-normal alignment of 'fast' axes in olivine crystals. However, to identify and delimit such a region we need to resolve anisotropic properties in depth as well as laterally. We conclude that corner flow cannot be assumed to be the dominant mechanism of the mantle wedge dynamics. Rather, it has to be shown to exist, for example through careful mapping of anisotropic indicators.

The corner-flow model implies steady-state subduction. However, Park *et al.* (2002) and Levin *et al.* (2002a) argue for recent (<2 Ma) catastrophic slab loss beneath the northern portion of the Kamchatka Slab. Near the Aleutian Junction, the Kamchatka Slab lacks both deep seismicity and the distinctive fast seismic wave speed that indicates the presence of cool dense descending oceanic lithosphere. This motivates the hypothesis for the loss of the slab edge via a convective instability. Loss of the slab edge would be followed by asthenospheric rebound. Quaternary volcanism in the interior of central Kamchatka contains alkaline basalts, often associated with a small-degree of partial melting of upwelling asthenosphere. The Kamchatka Slab has a shallower dip near the Aleutian Junction (35° versus 55°), which Park *et al.* (2002) argues is a transient response to either the loss of a deep-slab load or to asthenospheric flow from the Pacific to the Eurasian side of the plate boundary. Given these observations and hypotheses, it is not surprising that simple corner flow in the supraslab wedge fails to explain splitting data in the northern part of our study area.

If the shallow dip of the northernmost Kamchatka slab is a recent development, it would plausibly have induced a strong, but variable, anisotropic fabric as the supraslab mantle flowed up and away from the rising slab. The upward component of this mantle flow may be responsible for the unusually vigorous magmatism of the Klyuchevshoy volcanic centre, most of which is estimated to be Quaternary and Holocene in age (Erlich & Gorshkov 1979). The horizontal flow component may be responsible for the local *S* splitting, its strength as well as its complex geometry.

### SUMMARY

A combined data set from portable and permanent networks on Kamchatka between 1996 and 2001 provides dense sampling of the seismic anisotropy beneath the peninsula, and reveals lateral heterogeneity in shear wave splitting values. Splitting measurements vary from non-resolvable ('NULL') to unambiguous delays of nearly 1.0 s, with the majority of resolved splitting delays falling between 0.2 and 0.6 s. Approximately one-third of the analysed local *S* waves yield 'NULL' measurements.

Along the volcanic front, the southern part of the peninsula is characterized by nearly trench-normal alignment of the fast shear wave speed, while further towards the junction with the Aleutian Arc the pattern of fast polarization is complex. Near the northern edge of the subducting slab fast shear wave speed indicators rotate to a nearly north-south orientation, but show spatial variation. In the central part of the study area we find a region with very low, or non-existent, birefringence. Speculatively, this lack of birefringence may reflect a volume of supraslab mantle that lies between two deformation regimes, steady-state corner flow near Petropavlovsk and a transient flow away from the rising edge of the Kamchatka Slab beneath the Klyuchevskoy volcanic centre and the Aleutian Junction. Observations in the interior of the Kamchatka Peninsula generally display trench-parallel fast directions. This suggests that the supraslab mantle flow induced by shear coupling to the descending slab is limited in spatial extent, reaching no farther inland than the volcanic arc.

We do not observe systematic depth dependence of splitting time delays, or of measurement quality, either in the cumulative data set or in individual sets of observations at coastal stations. GSN station PET exhibits lateral variation in splitting parameters that appears related to the presence of an active volcanic centre to the north of the station. Events to the south of PET suggest an area of coherent anisotropy consistent with a 2-D corner flow in the mantle wedge. Events to the north of PET, near the volcanic centre, return inconsistent anisotropy indicators, as well as many NULL measurements.

## ACKNOWLEDGMENTS

Data used in this work came from a seismic network operated by the Kamchatka Experimental-Methodical Seismological Department, the Global Seismic Network and the temporary deployment of seismic sensors supplied by the PASSCAL pool. Some of the data were provided with assistance from the IRIS Data Management Center. Discussions with William Menke helped us devise a data quality ranking scheme. Reviews by Matthew Fouch, Rob van der Hilst and an anonymous reviewer contributed significantly to the overall quality of this manuscript. This work was supported by NSF grant EAR0106867. GMT software (Wessel & Smith 1991) was extensively used in the preparation of images.

## REFERENCES

- Aharonov, E., Whitehead, J.-A., Kelemen, P.-B. & Spiegelman, M., 1995. Channeling instability of upwelling melt in the mantle, *J. geophys. Res. B, Solid Earth Planets*, **100**(10), 20433–20450.
- Ando, M. & Ishikawa, Y., 1980. S-wave anisotropy in the upper mantle under a volcanic area in Japan, *Nature*, **286**, 43–46.
- Ando, M., Ishikawa, Y. & Yamazaki, F., 1983. Shear wave polarization anisotropy in the upper mantle beneath Honshu, Japan., *J. geophys. Res. B*, **88**(7), 5850–5864.
- Audoine, E., Savage, M.K. & Gledhill, K., 2000. Seismic anisotropy from local earthquakes in the transition region from a subduction to a strike-slip plate boundary, New Zealand, *J. geophys. Res. B, Solid Earth Planets*, **105**(4), 8013–8033.
- Bender, H., Levin, V. & Menke, W., 2004. Seismic anisotropy in the upper mantle beneath Adak Island records relative plate motion, *Eos, Trans. Am. geophys. Un., Joint Assembly Suppl.*, **85**(17), abstract S51B-07.
- Ben-Ismaïl, W. & Mainprice, D., 1998. An olivine fabric database; an overview of upper mantle fabrics and seismic anisotropy, *Tectonophysics*, **296**(1–2), 145–157.
- Bowman, J.R. & Ando, M.A., 1987. Shear wave splitting in the upper mantle wedge above the Tonga subduction zone, *Geophys. J. R. astr. Soc.*, **88**, 25–41.
- Buttles, J. & Olson, P., 1998. A laboratory model of subduction zone anisotropy, *Earth Planet. Sci. Lett.*, **164**, 245–262.
- Christensen, N.I., 1984. The magnitude, symmetry and origin of upper mantle anisotropy from fabric analyses of ultramafic tectonites, *Geophys. J. R. astr. Soc.*, **76**, 89–111.
- Crampin, S., 1977. Seismic wave propagation in anisotropic media; I, Computations, *Geophys. J. R. astr. Soc.*, **49**(1), 303.
- Erlich, E.N. & Gorshkov, G.S. (eds.), 1979. Quaternary volcanism and tectonics in Kamchatka, *Bull. Volcanol.*, **42**, 1–298.
- Fedotov, S.A. & Slavina, L.B., 1968. Estimation of longitudinal wave velocities in the upper mantle beneath north-western part of the Pacific and Kamchatka, *Izv. Akad. Nauk SSSR, Fiz. Zemli*, **2**, 8–31 (in Russian).
- Fischer, K.M. & Yang, X., 1994. Anisotropy in Kuril-Kamchatka subduction zone structures, *Geophys. Res. Lett.*, **21**(1), 5–8.
- Fischer, K.M., Fouch, M., Wiens, D. & Boettcher, M., 1998. Anisotropy and flow in Pacific subduction zone back-arcs, *Pure appl. Geophys.*, **151**, 463–475.
- Fischer, K.M., Parmentier, E.M., Stine, A.R. & Wolf, E.R., 2000. Modeling anisotropy and plate driven flow in the Tonga subduction zone back arc, *J. geophys. Res.*, **105**, 16 181–16 191.
- Fouch, M. & Fischer, K.M., 1996. Mantle anisotropy beneath Northwest Pacific subduction zones, *J. geophys. Res. B, Solid Earth Planets*, **101**(7), 15 987–16 002.
- Gorbatov, A., Kostoglodov, V., Suarez, G. & Gordeev, E., 1997. Seismicity and structure of the Kamchatka subduction zone, *J. geophys. Res.*, **102**, 17 883–17 898.
- Gorbatov, A., Dominguez, J., Suarez, G., Kostoglodov, V., Zhao, D. & Gordeev, G., 1999. Tomographic imaging of the P-wave velocity structure beneath the Kamchatka Peninsula, *Geophys. J. Int.*, **137**, 269–279.
- Hall, C.E., Fischer, K.M., Parmentier, E.M. & Blackman, D.K., 2000. The influence of plate motions on three dimensional back arc mantle flow and shearwave splitting, *J. geophys. Res.*, **105**, 28009–28033.
- Holtzmann, B.K., Kohlstedt, D.L., Zimmerman, M.E., Heidelbach, F., Hiraga, T. & Hustoft, J., 2003. Melt segregation and strain partitioning: Implications for seismic anisotropy and mantle flow, *Science*, **301**, 1227–1230.
- Ida, Y., 1983. Convection in the mantle wedge above the slab and tectonic processes in subduction zones, *J. geophys. Res.*, **88**, 7449–7456.
- Jung, H. & Karato, S.I., 2001. Water-induced fabric transitions in olivine, *Science*, **293**, 1460–1462.
- Kaminski, E. & Ribe, N.M., 2001. A kinematic model for recrystallization and texture development in olivine polycrystals, *Earth planet. Sci. Lett.*, **189**, 253–267.
- Kaneshima, S. & Silver, P.G., 1992. A search for source side mantle anisotropy, *Geophys. Res. Lett.*, **19**(10), 1049–1052.
- Korenaga, J. & Kelemen, P., 1998. Melt migration through the oceanic lower crust: a constraint from melt percolation modeling with finite solid diffusion, *Earth planet. Sci. Lett.*, **156**(1–2), 1–11.
- Krasnova, M.A. & Chesnokov, E.M., 1998. P-wave polarization changes in Kamchatka crust based on local seismograms, *Vulkanol. Seysmol.*, **4–5**, 138–148.
- Leat, P.T., Livermore, R.A., Millar, I.L. & Pearce, J.A., 2000. Magma supply in back-arc spreading centre segment E2, East Scotia Ridge, *J. Petrol.*, **41**, 845–866.
- Levin, V. & Okaya, D., 2003. Cause and effect: Seismic anisotropy measurements using full wavefield simulations in realistic mantle flow models, *EOS Trans. AGU*, **84**(46), Full Mtg. Supplement, Abstract T52E-02.
- Levin, V., Menke, W. & Park, J., 1999. Shear-wave splitting in Appalachians and Urals: a case for multilayered anisotropy, *J. geophys. Res.*, **104**, 17 975–17 994.
- Levin, V., Shapiro, N., Park, J. & Ritzwoller, M., 2002a. Seismic evidence for catastrophic slab loss beneath Kamchatka, *Nature*, **418**, 763–767.
- Levin, V., Park, J., Lees, J., Brandon, M.T., Peyton, V., Gordeev, E. & Ozerov, A., 2002b. Crust and upper mantle of Kamchatka from teleseismic receiver functions, *Tectonophysics*, **358**, 233–265.
- Luneva, M.N., Droznin, D.V. & Ovchinnikov, V.E., 2000. Shear wave splitting study on Kamchatka Peninsula from earthquakes of 1998, *Pacific Geol.*, **19**, 78–90 (in Russian).
- Margheriti, L., Nostro, C., Cocco, M. & Amato, A., 1996. Seismic anisotropy beneath the Northern Apennines (Italy) and its tectonic implications, *Geophys. Res. Lett.*, **23**, 2721–2724.
- Margheriti, L., Lucente, F.P. & Pondrelli, S., 2003. SKS splitting measurements in the Apenninic-Tyrrhenian domain (Italy) and their relation with lithospheric subduction and mantle convection, *J. geophys. Res.*, **108**(B4), doi: 10.1029/2002JB00179.
- Mehl, L., Hacker, B.R., Hirth, G. & Kelemen, P.B., 2003. Arc-parallel flow within the mantle wedge: Evidence from the accreted Talkeena arc, south central Alaska, *J. geophys. Res.*, **108**, B8, 2375, doi:10.1029/2002JB002233.
- Menke, W. & Levin, V., 2003. A Waveform-based method for interpreting SKS splitting observations, with application to one and two layer anisotropic Earth models, *Geophys. J. Int.*, **154**, 1–14.

- Park, J. & Levin, V., 2002. Seismic anisotropy: tracing plate dynamics in the mantle, *Science*, **296**, 485–489.
- Park, J., Levin, V., Brandon, M.T., Lees, J.M., Peyton, V., Gordeev, E. & Ozerov, A., 2002. A dangling slab, amplified arc volcanism, mantle flow and seismic anisotropy near the Kamchatka plate corner, in: *Plate Boundary Zones*, AGU Geodynamics Series 30, pp. 295–324, ed. Stein, S. and Freymuller, J. American Geophysical Union, Washington, DC.
- Peacock, S.M. & Wang, K., 1999. Seismic consequences of warm versus cool subduction metamorphism: examples from southwest and northeast Japan, *Science*, **286**, 937–939.
- Peyton, V., Levin, V., Park, J., Brandon, M.T., Lees, J., Gordeev, E. & Ozerov, A., 2001. Mantle flow at a slab edge: seismic anisotropy in the Kamchatka region, *Geophys. Res. Lett.*, **28**, 379–382.
- Pollet, J., Silver, P.G., Beck, S., Wallace, T., Zandt, G., Ruppert, S., Kind, R. & Rudloff, A., 2000. Shear wave anisotropy beneath the Andes from the BANJO, SEDA, and PISCO experiments, *J. geophys. Res., Solid Earth Planets.*, **105**(3), 6287–6304.
- Rumpker, G. & Silver, P.G., 1998. Apparent shear-waves splitting parameters in the presence of vertically varying anisotropy, *Geophys. J. Int.*, **135**, 790–800.
- Saltzer, R.L., Gaherty, J.B. & Jordan, T.H., 2000. How are shear-wave splitting measurements affected by variations in the anisotropy with depth?, *Geophys. J. Int.*, **141**, 374–390.
- Savage, M.K., 1999. Seismic anisotropy and mantle deformation: what we have learned from shear wave splitting, *Rev. Geophys.*, **37**, 65–105.
- Shapiro, N.M., Gorbato, A.V., Gordeev, E. & Dominguez, J., 2000. Average shear-velocity structure of the Kamchatka peninsula from the dispersion of surface waves, *Earth Planets Space*, **52**, 573–577.
- Shimizu, J., Nakajima, J. & Hasegawa, A., 2003. Shear-wave polarization anisotropy in the mantle wedge beneath the southern part of Tohoku, Japan, *EOS, Trans. Am. geophys. Un., Fall Meet. Suppl.*, **84**(46), abstract S31C-0779.
- Silver, P.G., 1996. Seismic anisotropy beneath the continents: probing the depths of geology, *Ann. Rev. Earth Planet. Sci.*, **24**, 385–432.
- Silver, P.G. & Chan, W.W., 1991. Shear-wave splitting and subcontinental mantle deformation, *J. geophys. Res.*, **96**, 16 429–16 454.
- Silver, P.G. & Savage, M.K., 1994. The interpretation of shear wave splitting parameters in the presence of two anisotropic layers, *Geophys. J. Int.*, **119**, 949–963.
- Smith, G.P., Wiens, D.A., Fischer, K., Dorman, L., Webb, S. & Hildebrand, J., 2001. A complex pattern of mantle flow in the Lau backarc, *Science*, **292**, 713–716.
- Stern, R.J., 2002. Subduction zones, *Rev. Geophys.*, **40**(4), 1012, doi:10.1029/2001RG000108.
- Vinnik, L.P., Kosarev, G.L. & Makeyeva, L.I., 1984. Anisotropy of the lithosphere according to the observations of SKS and SKKS waves, *Dokl. Akad. Nauk SSSR*, **278**(6), 1335–1339 (in Russian).
- Weimer, S., Tytgat, G., Wyss, M. & Duenkel, U., 1999. Evidence for shear-wave anisotropy in the mantle wedge beneath south-central Alaska, *Bull. seism. Soc. Am.*, **89**, 1313–1322.
- Wessel, P. & Smith, W.H.F., 1991. Free software helps map and display data, *EOS, Trans. Am. geophys. Un.*, **72**, 441.
- Yang, X., Fischer, K.M. & Abers, G., 1995. Seismic anisotropy beneath the Shumagin Islands segment of the Aleutian-Alaska subduction zone, *J. geophys. Res. B, Solid Earth Planets*, **100**(9), 18 165–18 177.
- Zhang, S. & Karato, S., 1995. Lattice preferred orientation of olivine aggregates deformed in simple shear, *Nature*, **375**, 774–777.

## APPENDIX

Formal errors of shear wave splitting values determined for individual observations are commonly evaluated by examining the shape of the misfit surface on which the measurement occupies a minimum. Interpreting the shape of the surface in terms of statistical uncertainties is not straightforward, as it requires additional assumptions about the error structure in the data. Levin *et al.* (1999) describe a method for estimating formal errors for measurements performed using a cross-correlation estimator. This technique appears to work well for teleseismic SKS phases where the initial polarization of the wave is known, and the period of the wave is typically much longer than the value of the delay.

In this paper we deal with *S* waves of unknown initial polarization, and with a period that is often comparable to the delay. Furthermore, we are cognizant of the ‘effective’ nature of the measurements. We note that the meaning of a formal error in the value of a single fast direction is vague if the waveform has sampled two or more anisotropic regions.

Most importantly, we found that formal errors determined for individual measurements proved to be poor predictors of the other metric that we used to rank our observations—that of a misfit between two distinct techniques for shear wave splitting estimation. One expects that small formal errors correspond to data examples where different splitting estimators agree well, and large formal errors correspond to data where there is disagreement between methods. Unfortunately, these expectations are not sustained.

In Fig. A1 we document the fact that for the ‘BEST’ quality observations the value of the formal error and the misfit between techniques are very close. However, for observations we designated ‘FAIR’, and even more dramatically for those designated ‘NULL’, we see a large discrepancy between relatively small formal errors and the large values of misfit. Thus good agreement between splitting estimators usually implies small formal errors, but the converse is not true.

Given the above considerations we believe that misfits of the two techniques are a much better indicator of the quality of a particular measurement.

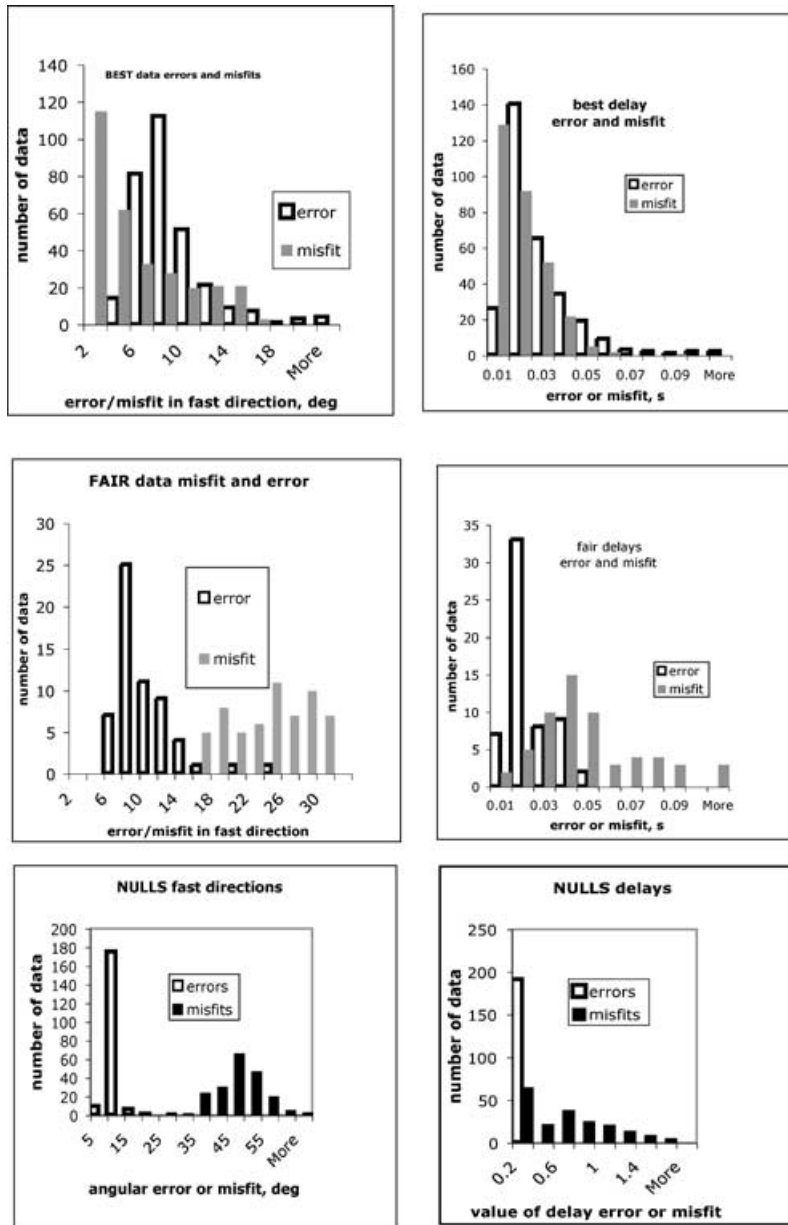


Figure A1. Histograms comparing values of formal errors and misfits between two splitting estimators for three classes of data (BEST, FAIR and NULL).